Experimental comparison of induction control methods for wind farm power maximization on a scaled two-turbine setup

Van Der Hoek, Daan; Ferreira, Carlos Simão; Van Wingerden, Jan Willem

DOI
10.1088/1742-6596/2767/9/092064

Publication date
2024

Document Version
Final published version

Published in
Journal of Physics: Conference Series

Experimental comparison of induction control methods for wind farm power maximization on a scaled two-turbine setup

Journal of Physics: Conference Series **2767** (2024) 092064 doi:10.1088/1742-6596/2767/9/092064

Experimental comparison of induction control methods for wind farm power maximization on a scaled two-turbine setup

Daan van der Hoek[1], Carlos Simão Ferreira[2], and Jan-Willem van Wingerden[1]

[1] Delft Center for Systems and Control, Faculty of Mechanical Engineering, Delft University of Technology, Delft, The Netherlands
[2] Wind Energy Section, Department of Flow Physics and Technology, Faculty of Aerospace Engineering, Delft University of Technology, Delft, The Netherlands

E-mail: d.c.vanderhoek@tudelft.nl

Abstract. Induction control methods offer a potential solution to minimizing wake effects that occur in large wind farms. This paper presents an experimental study on multiple induction control methods for wind farm power maximization. Wind tunnel experiments were conducted on two aligned scaled wind turbines. The upstream turbine was operated with static induction control, periodic dynamic induction control with collective pitch actuation, and dynamic individual pitch control (the helix approach). All wind farm control implementations were compared to a baseline case, which optimized the individual power extraction of both turbines. Tomographic particle image velocimetry was used to measure the wake of the upstream turbine. Based on turbine measurements, grid searches were employed to discover the optimal frequency and amplitude of the pitch actuation in the dynamic induction control cases. While static induction control showed increased wake velocities in the near wake, it did not provide an overall increase in power production of the two-turbine array. Dynamic induction control methods, especially the helix approach in the counterclockwise direction, were seen to significantly increase the total power output compared to the baseline control case. However, this improvement came with a larger amount of pitch actuation and increased fatigue loading of structural components in the fore-aft direction.

1. Introduction

Conventional operation of large wind turbine arrays inevitably leads to significant losses in energy capture due to wake effects [1]. Using wind farm flow control (WFFC), wind turbine wakes can be manipulated to partially mitigate these negative effects. Within the field of wind farm flow control, we distinguish between *wake steering control*, *static induction control* (SIC), and *dynamic induction control* (DIC) methods [2]. The latter two employ static or dynamic adjustments of either the tip speed ratio or blade pitch angle, to obtain a lower velocity deficit in the wake, or increase wake mixing, respectively. Ideally, the losses that result from operating the upstream turbine at sub-optimal conditions, are compensated by increased performance of downstream turbines.

While static induction control has the additional benefit of reduced structural fatigue loading [3], multiple studies have indicated that a positive impact on power performance is

small for closely spaced turbines [4, 5] and non-existent for larger turbine spacing [6, 7]. Dynamic induction control methods have shown more promising results when turbines are spaced further apart. Large eddy simulations of a wind farm incorporating a sinusoidal variation on the thrust force showed increased wake mixing, resulting in improved overall power performance [8]. Wind tunnel experiments that replicated this sinusoidal variation in thrust by periodically adjusting the collective blade pitch angle revealed similar performance [7]. A variation of dynamic induction control, called the *helix approach*, incorporates individual pitch control (IPC) to induce a helical velocity profile in the wake [9]. This method combines wake deflection with improved wake mixing to make it more effective than periodic DIC. Recent wind tunnel tests exploring the potential of the helix approach showed its effectiveness for maximizing the power of a two-turbine array [10, 11].

The different induction control methods mentioned earlier have previously been evaluated in a high-fidelity simulation environment [9]. In that particular study, the authors compared static induction control to periodic dynamic induction control (PDIC) and the helix approach on a two-turbine array with 5-diameter (D) spacing. The DIC implementations were evaluated for a single frequency and two different amplitudes. The results showed an increase in overall generated power for each of the DIC methods, while SIC resulted in a small net power loss. However, these power gains were achieved through a large increase in pitch actuation, especially for the helix case, and resulted in increased fatigue loading of the blades and tower [12].

The main contribution of this paper is a comparison of SIC and DIC methods on an experimental scaled two-turbine setup. Power measurements from both turbines were used to determine the optimal frequency and pitch amplitude for dynamic control. Strain gauge measurements at the tower base were used to obtain fatigue loading trends for each of the methods. Furthermore, tomographic particle image velocimetry (PIV) was employed to measure the wake of the actuated turbine for a subset of operational settings. This provided a direct comparison of the methods at different distances in the wake.

The paper is structured as follows. Section 2 describes the experiment setup including the wind tunnel, the wind turbine model, and the PIV setup. The experimental results are subsequently presented in Section 3. The paper is concluded in Section 4.

2. Experiment setup

The experiments presented in this paper were carried out at a closed circuit open jet wind tunnel with dimensions of 2.85 m by 2.85 m. The wind tunnel was operated at a constant wind speed of $U_\infty = 5\,\mathrm{m\,s^{-1}}$, with a maximum turbulence intensity of 2 %.

The experiment used two MoWiTO-0.6 wind turbines with a diameter of $D = 0.58\,\mathrm{m}$ and collective pitch capabilities [13]. The pitching mechanism of the upstream turbine was modified with a swashplate that allowed cyclic individual pitch control, which is required to apply the helix approach [11]. The turbines were set apart by a distance of $5\,D$, similar to comparable studies [9]. Strain gauges were applied at the tower base of each turbine to record the tower bending moment and reconstruct the thrust force. Both turbines were controlled through a *dSPACE MicroLabBox*, which recorded turbine output signals such as rotor speed, generator torque, pitch stepper motor encoders, and tower strain signals at a frequency of $f_s = 2\,\mathrm{kHz}$.

The upstream turbine (T1) was operated at a constant tip-speed ratio of $\lambda = 5$, to limit the effect of rotor speed changes on thrust force. The downstream turbine (T2) was regulated with the $K\Omega^2$-control law, which uses a constant K to operate the turbine at the optimal settings using the rotor speed measurement Ω [14]. The optimal pitch angle for the turbines was determined experimentally at the start of the measurement campaign at $\theta = 10°$. In this case, a pitch angle of 0° refers to the most outward position the blades can attain. The resulting power and thrust coefficients are presented in Figure 1.

During the experimental campaign, we considered four induction control methods and

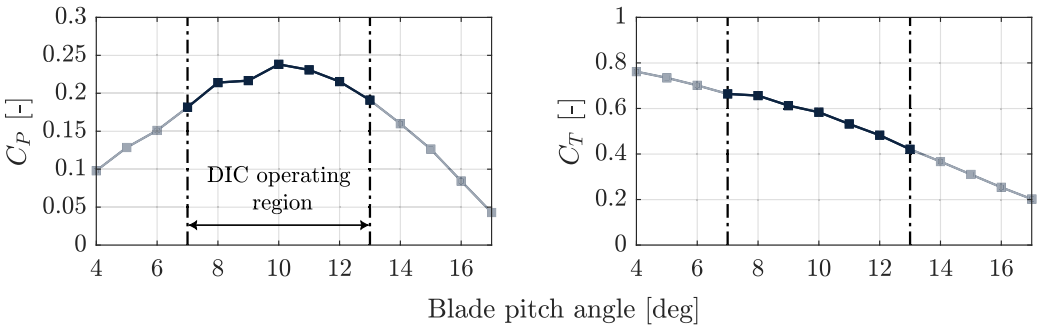

Figure 1. Experimentally determined power (C_P) and thrust (C_T) coefficients for a range of pitch angles. The dash-dotted lines mark the range of pitch angles that will be applied with the implementation of the different induction control methods.

compared these to a baseline measurement that consisted of running the upstream turbine with the optimal operating settings. Static induction control was implemented through a constant pitch angle offset of 2° from the optimal pitch angle. The other considered methods were periodic dynamic induction control, the clockwise (CW) helix approach, and the counterclockwise (CCW) helix approach. The direction of the helix approach corresponds to the direction the wake deficit is moving when viewed from in front of the turbine.

A range of pitch amplitudes and frequencies were considered to determine the optimal settings for these dynamic implementations, as will be shown in Section 3. The excitation frequency f_e is based on the dimensionless Strouhal number

$$\mathrm{St} = \frac{f_e D}{U_\infty}, \tag{1}$$

with rotor diameter D and freestream inflow velocity U_∞. For the helix case, f_e refers to the frequency at which the yaw and tilt moment are varied over time. The actual pitch frequency to achieve this is given by $f_\theta = f_r \pm f_e$, with f_r referring to the rotational frequency of the turbine. For the CW helix implementation, f_e is subtracted from f_r, and vice versa for the CCW method. An example of the different WFFC strategies in terms of the applied pitch angles is provided in Figure 2. The figure shows the increased pitch rate of the helix approach compared to PDIC. Furthermore, we observe that none of the pitch signals have a constant amplitude over time. This is due to the implementation of the swashplate, which doesn't allow direct control of each of the blades. In the remainder of the paper, the pitch amplitude will be expressed as the average pitch amplitude over a single excitation cycle.

In addition to the turbine measurements, the flow behind turbine T1 was recorded using tomographic PIV. The PIV setup consisted of a seeding rake situated at the outlet of the open jet, that released neutrally buoyant helium-filled soap bubbles into the flow [15]. Following illumination by two LED panels, the soap particles were recorded by four *Photron FASTCAM SA1.1* high-speed cameras, operating at a framerate of 500 frames/s and at a resolution of 1024 by 1024 pixels. The PIV data was subsequently processed with *LaVision's DaVis 10* software to reconstruct the particles in the flow over time. Finally, time-averaged three-dimensional flow fields were obtained by mapping the particle data onto a Cartesian grid with a resolution of 10 mm. An overview of the experiment setup with all the relevant dimensions is given in Figure 3. It also shows how the PIV setup was moved to capture multiple sections of the wake of T1. The measurement setup was the same as presented in [11], additional information can be found there.

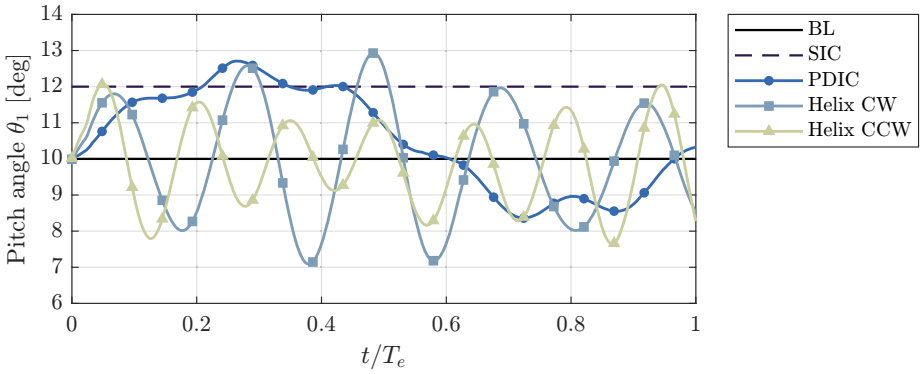

Figure 2. Comparison of the pitch angles for different induction control methods. The pitch angles of the DIC methods are given for a single excitation cycle at the same frequency, as expressed by time t normalized over one excitation period T_e.

3. Measurement results

3.1. Optimal dynamic induction control settings

Grid searches were performed for all DIC methods with different Strouhal numbers and pitch amplitudes to determine the optimal settings. The results of the grid searches are presented in Figure 4, which is split into three parts corresponding to the power of turbine T1, T2, and the combined power of the two turbines. The maximum amplitudes and frequencies differed between the methods as they were limited by the stepper motors driving the pitching mechanism. The performance of the WFFC strategies was compared to a baseline control case, where both turbines tried to maximize their power output.

From Figure 4, it becomes apparent that the power output of turbine T1 decreased for increasing pitch amplitudes, while it was less sensitive to a change in frequency. Furthermore, the helix method resulted in higher power losses than PDIC. Based on the measurements from T2, we observe improved wake recovery compared to the baseline case for all DIC methods. However, both implementations of the helix approach were a lot more effective than PDIC. Taking the sum of both turbine power measurements results in the bottom row of the figure. In the case of PDIC, the total power is approximately equal to the baseline case. The loss of power

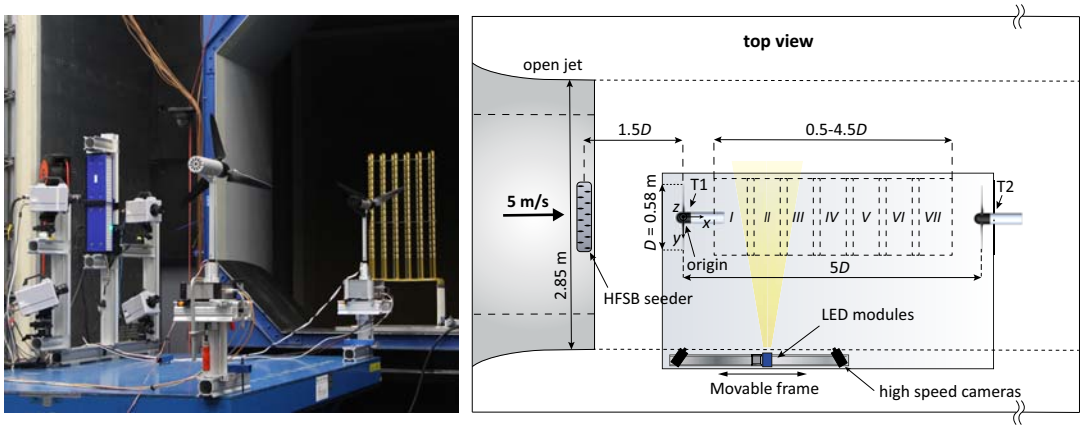

Figure 3. Overview of the experimental setup, highlighting the different components and the measured sections of the wake [11].

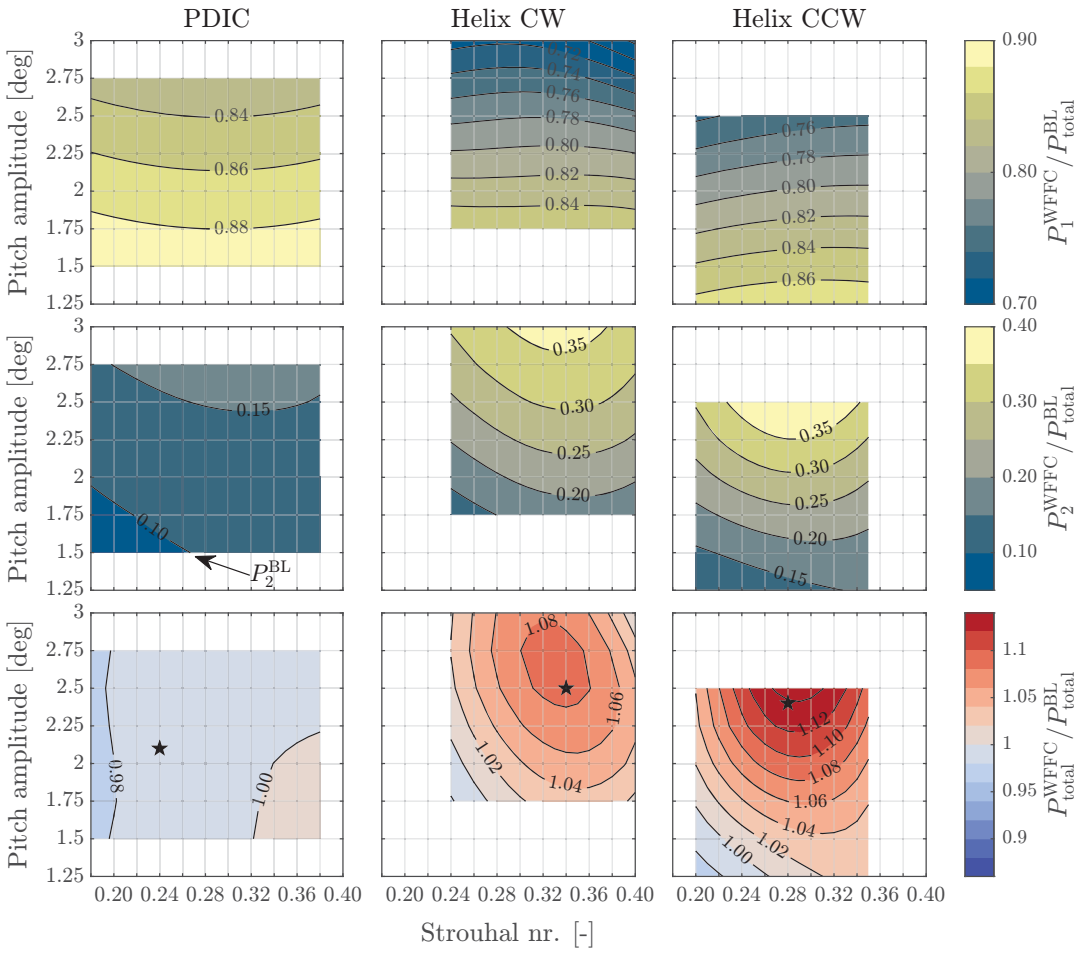

Figure 4. Grid search results of the total power gain for different pitch amplitudes and frequencies (expressed by St) for turbine T1 (top), T2 (middle), and the overall power $P_{\mathrm{total}}^{\mathrm{WFFC}}$(bottom). All power measurements were normalized with the total baseline power $P_{\mathrm{total}}^{\mathrm{BL}}$. From left to right, we see the results of PDIC, the CW helix method, and the CCW helix method. The ⋆ symbol indicates the DIC settings that were implemented for the PIV measurements.

at T1 could not be compensated sufficiently by the performance increase of T2. Both helix cases show a significant increase in total power gain, with the CCW implementation being the most effective. We can also observe a difference in the optimal pitch amplitude and frequency between these two cases. The difference in performance between the helix cases is believed to be the result of the interaction with the natural counterclockwise rotation of the wake [16].

The improved power output with the helix cases comes at the expense of increased pitch actuation. To quantify the effect of increased pitch activity on the power gain, we normalize the results from Figure 4 with the distance the blades have traveled during pitching. The pitch distance s_θ is defined as

$$s_\theta(f_e, A_\theta) = \int_{t=0}^{t} |\dot{\theta}(t, f_e, A_\theta)| dt, \tag{2}$$

with pitching velocity $\dot{\theta}$, time t, and pitching amplitude A_θ. Next, we use the pitch distance where PDIC reached its optimal power gain to acquire the relative (non-dimensional) pitch

distance

$$\bar{s}_\theta(f_e, A_\theta) = \frac{s_\theta(f_e, A_\theta)}{\max_{f_e, A_\theta}\left(s_\theta^{\mathrm{PDIC}}\right)}. \tag{3}$$

Next, the total power gain from Figure 4 is divided by $\bar{s}_\theta$ to visualize the dependency of each DIC method on the amount of pitch actuation. In Figure 5, we now observe that the potential power gain of the helix approach is in a similar range as that of PDIC, and that the difference between the CW and CCW helix, at least from a control point of view, can be explained by the additional pitch actuation.

3.2. Structural loading trends with induction control

Besides the additional strain on the pitch bearings due to the higher pitching activity, DIC methods also introduce additional fatigue loading on multiple turbine components of both the upstream and downstream turbines [12, 17, 18]. In contrast, SIC has been shown to decrease these loads [4]. The scaled turbine models used in this experiment do not allow an accurate assessment of the lifetime structural fatigue loading due to DIC. However, the strain gauge measurements at the tower base provide an indication of the increase in fatigue loading for several components in the fore-aft direction (e.g., tower bending moment and blade root out-of-plane bending moment) compared to baseline operation. On the left-hand side of Figure 6, time series of the tower bottom bending moment are given for the two turbines. Both turbines experience an increased bending moment when DIC is active. Furthermore, the DIC methods are characterized by a cyclic loading component, especially in the case of PDIC.

The right-hand side of Figure 6 contains the corresponding power spectral density (PSD) of the tower bending moment. In the PSD of T1, a spike is visible at the 1P rotational frequency for all test cases. The PSD for SIC is seen to be slightly below baseline operation for the majority of frequencies. Each of the DIC cases contains large peaks at the pitch excitation frequencies and its 3P multiple. When considering the PSD of T2, we can observe the same f_e peaks, albeit smaller in magnitude compared to T1. Once more, an increase in magnitude is observed for all DIC methods, while SIC is either below or equal to the baseline case. In the frequency range between 5 and 10 Hz, some new peaks have emerged corresponding to the 1P rotational frequency of T2. The location of this peak is different for each case due to differences in inflow velocities that T2 was experiencing.

Based on the PSD of both turbines, it is evident that DIC methods significantly increase the structural fatigue loading in the fore-aft direction, most noticeably in the case of PDIC. These

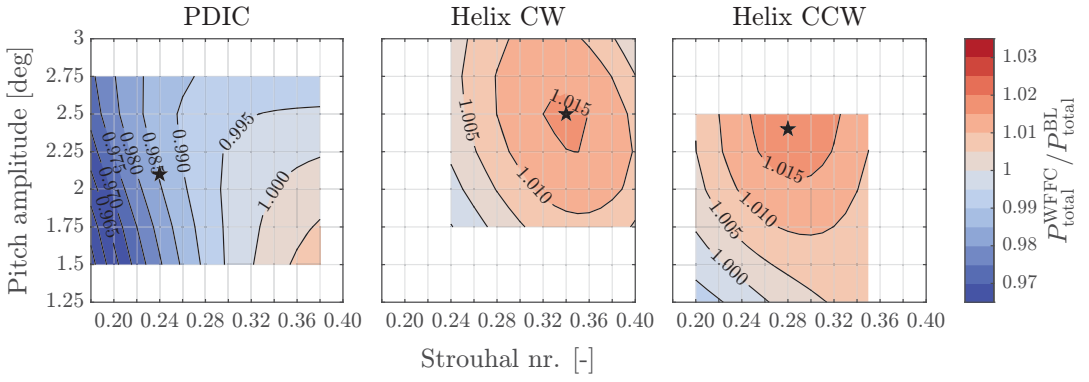

Figure 5. Grid search results of the total power gain as a function of amplitude and frequency (expressed by St). The measurements were normalized with the total baseline power $P_{\mathrm{total}}^{\mathrm{BL}}$, as well as the relative pitching distance $\bar{s}_\theta$.

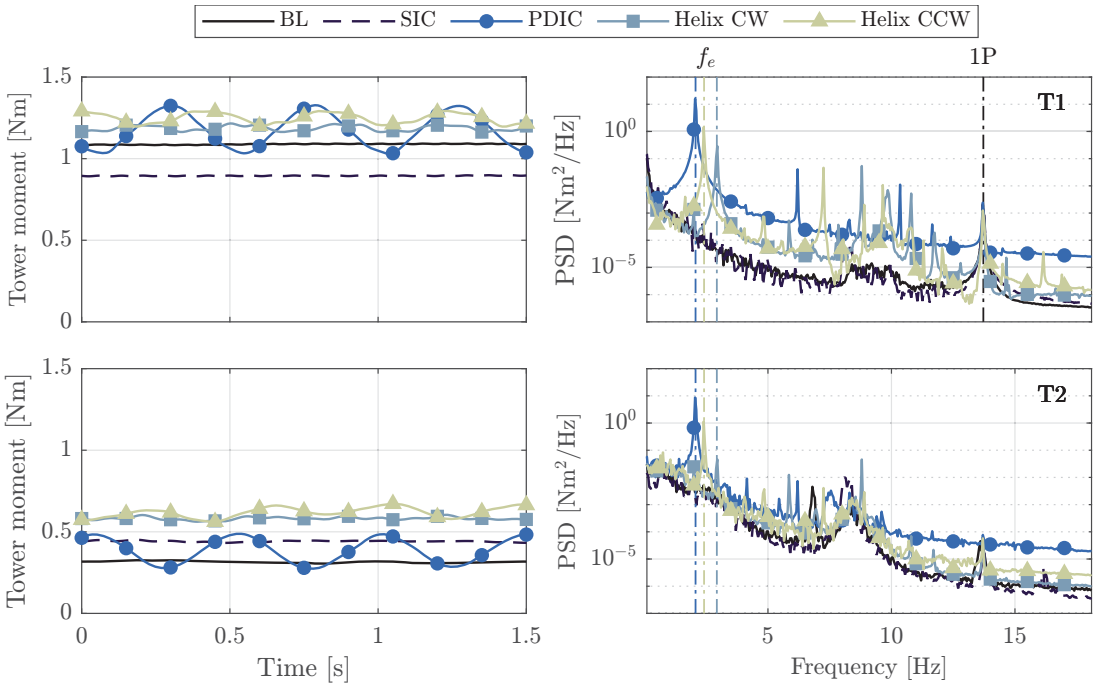

Figure 6. Time series of the tower bottom moment for both turbines under different induction control methods (left). The right-hand figures show the power spectral density of these time series. The dash-dotted lines indicate the excitation frequencies f_e of the DIC methods, as well as the 1P rotational frequency of turbine T1.

results are in line with previous studies on the impact of DIC on turbine fatigue loading [12, 17]. While the increased fatigue loading will harm turbine lifetime, it should be noted that DIC will only be active for short periods, and hence the impact on lifetime is expected to be small.

3.3. Wake velocity measurements

A set of WFFC settings was considered for the PIV measurements. The settings used for the DIC cases are marked in the bottom row of Figure 4. For the CW and CCW helix cases, frequencies and amplitudes close to the optimal settings were considered. For DIC, we chose a lower frequency closer to a previously reported optimum of St = 0.25 [7, 19].

Cross-stream slices of the streamwise velocity component u at four locations in the wake are presented in Figure 7. A clear distinction between baseline operation and SIC is noticeable, with the latter having a significantly smaller velocity deficit at all locations. In the case of PDIC, this difference is less clear. At distances of $x/D = 1$ and $x/D = 2$, both helix cases are still similar to the baseline case. Moving further downstream, the improved wake recovery of the helix approach becomes apparent. A direct comparison of all methods is provided in the final row of the figure, which shows the velocity deficit at hub height ($z/D = 0$). In the near wake, SIC seems to be the most effective method. Starting from $x/D = 3$, the CW and CCW helix start improving and at $x/D = 4$, the CCW helix is seen to surpass SIC. Furthermore, all DIC methods are characterized by a wider wake profile compared to the baseline and SIC cases. A slight increase in velocity deficit at $x/D = 4$ can also be remarked for some of the test cases. We believe this to be the result of the downstream turbine's induction zone.

The power signals that were collected during the PIV measurements were subsequently time-averaged to obtain Figure 8. Turbine T1 suffers from a loss in performance for all control methods, but most severely for the helix cases. Here, we observe a decrease in power of over

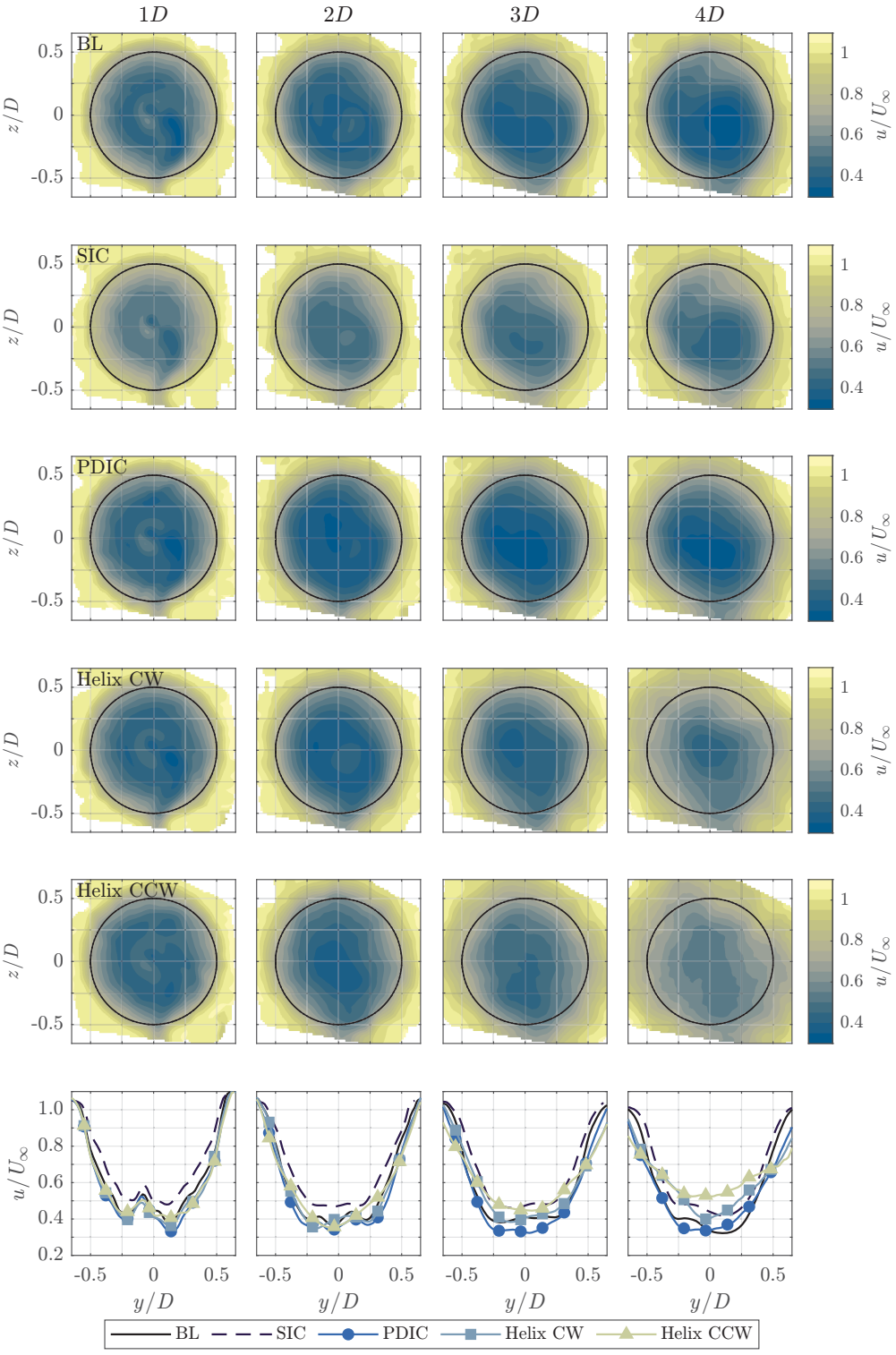

Figure 7. Cross-stream flow slices of the time-averaged normalized streamwise velocity u/U_∞ at distances x/D = 1–4 downstream. The velocity was normalized with the freestream inflow velocity $U_\infty = 5\,\mathrm{m\,s^{-1}}$. The bottom row compares the streamwise velocity profiles of the induction control methods at the respective locations in the wake.

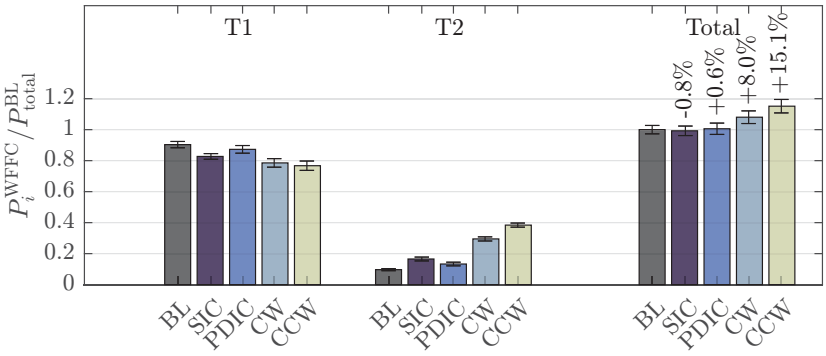

Figure 8. Averaged power output of turbines T1, T2 and sum of the two turbines for different induction control methods. The power was normalized with the overall total power production of the baseline control case $P_{\mathrm{total}}^{\mathrm{BL}}$. The error bars indicate $\pm 2\sigma$, with σ the standard deviation.

10% for a pitch amplitude of 2.5°. The decrease is more severe compared to simulation studies that consider utility-scale turbines [20]. This is the result of a steeper power curve (as seen in Figure 1), which is a characteristic of small-scale turbines. All control methods were able to decrease the wake velocity deficit at $x/D = 5$, resulting in more power generated by T2. Surprisingly, the power of T2 with SIC was higher than in the case of PDIC. With the helix cases, a significant increase in power was achieved for T2.

When considering the total power, we see that SIC was not able to compensate for the loss in power of T1. However, PDIC achieved a minor improvement in power production of 0.8%. This is contrary to the grid search results of Figure 4, which showed a small decrease in total power for the settings that were considered during the PIV measurements. However, Figure 8 results from several repetitions for each induction control case (corresponding to different wake measurement locations), and hence is deemed more reliable. The improved wake recovery achieved with the helix approach is more than sufficient to make up for the high power loss of T1.

The experiments presented in this paper were carried out under low turbulent conditions, with the turbulence intensity in the range of 2% [11]. Hence, the naturally occurring wake recovery that is driven by ambient turbulence intensity is less dominant compared to reality. While large eddy simulations have shown that the helix approach can still improve power performance in the case of a turbulent boundary layer [9, 20], the wake recovery due to the helix will become less pronounced for increasing turbulence intensity.

4. Conclusion

This paper provided a comparison of multiple induction control methods for maximizing the power of a two-turbine array in a wind tunnel. The methods that were considered consisted of static induction control with a blade pitch offset, periodic dynamic induction control with collective pitch actuation, and dynamic individual pitch control, also known as the helix approach. Grid searches were performed to determine the optimal pitching frequency and amplitude for the DIC methods. These grid searches visualized the effectiveness of the helix approach, and how this was mostly achieved through a major increase in pitch actuation, also compared to PDIC.

Besides the significant additional loading on the pitch bearing mechanisms, all DIC methods were seen to increase the structural fatigue loading in the fore-aft tower bending moment. This was most noticeable in the PSD of the PDIC case. In contrast, SIC showed a lower PSD compared to the baseline case, indicating a decrease in fatigue loading for this control method.

Time-averaged PIV measurements were subsequently presented, which showed the dominance

of SIC in the near wake ($x/D < 3$). However, for the mid-wake ($x/D \approx 4$), the helix method surpassed all other methods. This was also visible when considering the time-averaged power signals of the PIV measurements, which demonstrated the superiority of the helix method for increasing the power gain of a two-turbine array.

References

[1] P. Veers *et al.*, "Grand challenges in the design, manufacture, and operation of future wind turbine systems," *Wind Energy Science*, vol. 8, pp. 1071–1131, 7 2023.
[2] J. Meyers *et al.*, "Wind farm flow control: Prospects and challenges," *Wind Energy Science*, vol. 7, pp. 2271–2306, 11 2022.
[3] P. A. Fleming, J. Aho, A. Buckspan, E. Ela, Y. Zhang, V. Gevorgian, A. Scholbrock, L. Pao, and R. Damiani, "Effects of power reserve control on wind turbine structural loading," *Wind Energy*, vol. 19, pp. 453–469, 3 2016.
[4] D. van der Hoek, S. Kanev, J. Allin, D. Bieniek, and N. Mittelmeier, "Effects of axial induction control on wind farm energy production - a field test," *Renewable Energy*, vol. 140, pp. 994–1003, 2019.
[5] E. Bossanyi and R. Ruisi, "Axial induction controller field test at Sedini wind farm," *Wind Energy Science*, vol. 6, pp. 389–408, 3 2021.
[6] J. Annoni, P. M. O. Gebraad, A. K. Scholbrock, P. A. Fleming, and J. W. van Wingerden, "Analysis of axial-induction-based wind plant control using an engineering and a high-order wind plant model," *Wind Energy*, vol. 19, no. 6, pp. 1135–1150, 2016.
[7] J. A. Frederik, R. Weber, S. Cacciola, F. Campagnolo, A. Croce, C. Bottasso, and J. W. van Wingerden, "Periodic dynamic induction control of wind farms: proving the potential in simulations and wind tunnel experiments," *Wind Energy Science*, vol. 5, pp. 245–257, 2 2020.
[8] W. Munters and J. Meyers, "Towards practical dynamic induction control of wind farms: Analysis of optimally controlled wind-farm boundary layers and sinusoidal induction control of first-row turbines," *Wind Energy Science*, vol. 3, pp. 409–425, 1 2018.
[9] J. A. Frederik, B. M. Doekemeijer, S. P. Mulders, and J. W. van Wingerden, "The helix approach: using dynamic individual pitch control to enhance wake mixing in wind farms," *Wind Energy*, no. May, 2020.
[10] F. M. Heckmeier, *Multi-Hole Probes for Unsteady Aerodynamics Analysis*. PhD thesis, Technische Universität München, 2022.
[11] D. van der Hoek, B. V. den Abbeele, C. Simao Ferreira, and J. W. van Wingerden, "Maximizing wind farm power output with the helix approach: Experimental validation and wake analysis using tomographic particle image velocimetry," *Wind Energy*, 2024.
[12] J. A. Frederik and J. W. van Wingerden, "On the load impact of dynamic wind farm wake mixing strategies," *Renewable Energy*, vol. 194, pp. 582–595, 7 2022.
[13] J. Schottler, A. Hölling, J. Peinke, and M. Hölling, "Design and implementation of a controllable model wind turbine for experimental studies," *Journal of Physics: Conference Series*, vol. 753, no. 7, 2016.
[14] E. A. Bossanyi, "The Design of closed loop controllers for wind turbines," *Wind Energy*, vol. 3, pp. 149–163, 7 2000.
[15] F. Scarano, S. Ghaemi, G. C. A. Caridi, J. Bosbach, U. Dierksheide, and A. Sciacchitano, "On the use of helium-filled soap bubbles for large-scale tomographic PIV in wind tunnel experiments," *Experiments in Fluids*, vol. 56, 2 2015.
[16] M. Coquelet, J. Gutknecht, J. W. van Wingerden, M. Duponcheel, and P. Chatelain, "Dynamic individual pitch control for wake mitigation: Why does the helix handedness matter?," in *Journal of Physics: Conference Series*, 2024.
[17] A. A. van Vondelen, S. T. Navalkar, D. R. Kerssemakers, and J. W. van Wingerden, "Enhanced wake mixing in wind farms using the Helix approach: A loads sensitivity study," *2023 American Control Conference (ACC)*, pp. 831–836, 5 2023.
[18] S. Cacciola, A. Bertozzi, L. Sartori, and A. Croce, "On the dynamic response of a pitch/torque controlled wind turbine in a pulsating dynamic wake," in *Journal of Physics: Conference Series*, vol. 1618, IOP Publishing Ltd, 9 2020.
[19] D. van der Hoek, J. Frederik, M. Huang, F. Scarano, C. Simao Ferreira, and J. W. van Wingerden, "Experimental analysis of the effect of dynamic induction control on a wind turbine wake," *Wind Energy Science*, vol. 7, pp. 1305–1320, 6 2022.
[20] E. Taschner, A. A. W. van Vondelen, R. Verzijlbergh, and J. W. van Wingerden, "On the performance of the helix wind farm control approach in the conventionally neutral atmospheric boundary layer," *Journal of Physics: Conference Series*, vol. 2505, p. 12006, 2023.